THE JOURNAL OF PHYSICAL CHEMISTRY C

Article

Cite This: J. Phys. Chem. C 2018, 122, 22864−22875

pubs.acs.org/JPCC

Nanostructure and Dynamics of Humidified Nafion/Graphene-Oxide Composites via Molecular Dynamics Simulations

Georgios Kritikos,*[,†] Rakesh Pant,[‡] Soumyadipta Sengupta,[∥] Kostas Karatasos,*[,†,§] Arun Venkatnathan,[‡] and Alexey V. Lyulin[∥,⊥]

[†]Laboratory of Physical Chemistry, Department of Chemical Engineering, Aristotle University of Thessaloniki, 54124 Thessaloniki, Greece

[‡]Department of Chemistry and Centre for Energy Science, Indian Institute of Science Education and Research, Dr. Homi Bhabha Road, Pashan, Pune 411008, Maharashtra, India

[§]Institute of Electronic Structure and Laser, Foundation for Research and Technology—Hellas, P.O. Box 1527, 711 10 Heraklion, Crete, Greece

[∥]Theory of Polymers and Soft Matter, Department of Applied Physics, Technische Universiteit Eindhoven, P.O. Box 513, 5600 MB Eindhoven, The Netherlands

[⊥]Center for Computational Energy Research, Technische Universiteit Eindhoven, P.O. Box 6336, 5600 HH Eindhoven, The Netherlands

Supporting Information

ABSTRACT: In this work, we elucidated the nanostructure and dynamics of Nafion-doped graphene-oxide (GO) systems from molecular dynamics simulations at varying hydration levels and temperature. It was found that the presence of GO resulted in the formation of Nafion layers along a direction normal to the GO surface. Chain conformations in the Nafion layers close to the GO interface were characterized by a backbone preferably oriented parallel to the GO plane, whereas the size of the formed nanochannels was found to be commensurate to the average dimensions of the Nafion side chains. The mechanism of water cluster growth was found to change drastically upon introduction of Nafion chains, although addition of GO in the membranes did not impart further measurable changes at the examined temperatures. Hydronium ions were found to adsorb partly onto the GO surface, whereas the pertinent adsorption/desorption rate increased significantly with hydration. Translational dynamics of water molecules was much slower close to the GO surface compared to that at distances far from GO. In the temperature range examined, the dynamics of the effectively confined water molecules was found to follow an Arrhenius-like dependence. Water retention at the Nafion/GO interface appears only at high hydration levels of Nafion.

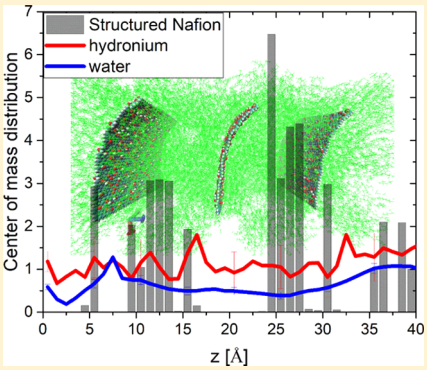

1. INTRODUCTION

Polymer electrolyte membrane (PEM) fuel cells have continued to generate a lot of attention because of their ability to generate electricity with minimal emissions.[1] A lot of work on PEMs have focused on perfluorosulfonic acid (PFSA) membranes as they offer high proton conductivity and high chemical and thermal stabilities with low permeability for fuel crossover. The effect of humidification on PFSA membranes has been explored by a variety of experimental techniques such as contact angle measurements,[2−4] atomic force microscopy,[5−8] electrochemical mass transport measurements,[9] and X-ray studies.[10] Experimental investigations were used to understand several properties such as surface morphology, membrane deformation, structure factor, scattering intensity, micelle orientation, and water uptake.

Complementary to experimental investigations, computational methods have provided several physical insights into the molecular level interactions, which influence the nanostructure and dynamics of hydrated PFSA membranes. Among the PFSA class of membranes, the noteworthy and the most widely investigated is the Nafion membrane. Several key findings on the structure and dynamics of a hydrated Nafion membrane from computer simulations have been reported. Vishnyakov and Neimark[11] studied microphase segregation in the Nafion membrane from molecular dynamics (MD) simulations and concluded that the proton conductivity of the membrane depends on hydration. Paddison,[12] using density functional theory calculations, showed that proton transfer from the sulfonic acid group in Nafion to water requires a minimum of three water molecules. In another work,[13] the authors showed that structural diffusion (Grotthuss diffusion[14]) can occur even with strong sulfonate−water interactions. The effect of

Received: July 25, 2018
Revised: September 16, 2018
Published: September 19, 2018

DOI: 10.1021/acs.jpcc.8b07170
J. Phys. Chem. C 2018, 122, 22864−22875

monomeric sequence on phase segregation and dynamics in hydrated Nafion was studied by Jang et al. using MD simulations. The authors concluded that transport of water molecules depends on the structural differences imposed by the monomeric sequence, and the diffusion of water molecules is larger in the dispersed sequence as compared to that in the blocky sequence.[15] Urata et al.[16] employed MD simulations and concluded that water preferably interacts with the sulfonate group of the side chain of PFSA membranes. The authors also reported an orientation of pendant side chains that is perpendicular to the polar/nonpolar backbone interface. Devanathan et al.[17−19] employed MD simulations to understand the nanostructure of Nafion membranes and the dynamics of water and hydronium ions. The authors concluded that hydronium ions play a significant role in modifying the hydrophilic phase near the pendant groups.[17] In another work, the authors have mentioned that water mainly interacts with the sulfonate groups and not with the ether or hydrophobic backbone of Nafion.[18] Further, the authors reported the diffusion coefficients for hydronium ions to be in close agreement with a quasi-elastic neutron scattering experimental study.[19] Cui et al.[20] explored hydrated Nafion using MD simulations and concluded that the system consists of hydrophobic domains due to the nonpolar backbone and hydrophilic regions with a heterogeneous distribution of water. Sunda and Venkatnathan investigated the effect of hydration and temperature on the side chains of three PFSA membranes (Nafion, Dow, and Aciplex). The authors noted that the presence of an extra ether oxygen in Nafion provides extra flexibility to the sulfonate groups, which assists in an enhanced interaction with the hydrophilic phase.[21]

Voth and co-workers[22] demonstrated the limitations of the classical description of the proton as hydronium by performing multistate empirical valence bond (MS-EVB) simulations. The authors also used the self-consistent iterative (SCI) MS-EVB method[23] to examine the solvation and transport properties of the sulfonate-hydronium ion pair in hydrated Nafion membranes. In another SCI-MS-EVB simulation study, the authors showed that sulfonate groups affect the direction of proton hopping.[24] The authors varied water from lower to higher content and observed a transition from undissociated sulfonic acid to localized hydronium ions and to delocalized hydronium ions ($H_5O_2^+$) at higher water content. Ilhan and Spohr[25] employed ab initio MD simulations to explore the structure and dynamics of water in two narrow cylindrical pores consisting of CF_3-CF_3 and sulfonic acid groups to mimic hydrated Nafion membranes.

The humidification of Nafion membrane is critical, as it affects the conductivity of a fuel cell. At temperatures above 80 °C or at low hydration levels, the conductivity reduces, and hence the membrane must be sufficiently hydrated to achieve high proton conductivity.[26] In a typical fuel cell, the supplied hydrogen gas is often humidified to enhance proton conductivity. However, the external humidification results in an increase in the size of the fuel cell, which is not desirable for portable applications.[27] To avoid external humidification, self-humidifying membranes have been explored, which utilize inorganic fillers. These inorganic fillers such as silica, titania, zirconia, iron oxides, carbon nanotubes, zeolites, and clay assist in water retention and enhance the proton-conducting properties and mechanical and thermal stabilities of the membrane.[28] Recently, Nafion/graphene-oxide (GO) composites have been explored as potential electrolytes. The choice of GO stems from properties such as large surface area, hydrophilic functional groups, mechanical strength, and chemical stability, which makes it an ideal candidate to form composite membranes.[29] Hayami et al.[30] demonstrated that the conductivity of GO could reach 10^{-2} S cm^{-1} and concluded that the hydrophilic groups of GO interact with the protons, which are propagated through the hydrogen-bonding network formed with the adsorbed water. Zarrin et al.[31] observed that the conductivity is enhanced when a Nafion membrane is doped with functionalized GO particles.

Water retention enhances proton conduction by the formation of proton transport channels, which also depends on the hydrophilic functional groups of the membrane. GO is known to assist in water retention because of the presence of epoxy and hydroxyl groups, which can form hydrogen bonds with water molecules. Devanathan et al.[32] investigated water interactions with GO at various hydration using MD simulations. The authors concluded that the diffusion of water molecules in GO is slower because of hydrogen-bonding interactions between the water molecules and hydroxyl groups of GO. Liu et al.[33] showed that the transport of water and other small molecules through graphene-based membranes depends on interlayer channels and functional groups.

Choi et al.[34] examined Nafion/GO composites for direct methanol fuel cell applications and concluded that the transport properties of the Nafion membrane were improved by the incorporation of GO. Enotiadis et al.[35] investigated Nafion/GO composites with GOs functionalized with hydrophilic groups such as $-SO_3H$, $-OH$ and $-NH_2$. The authors concluded that such hydrophilic groups in GO improved proton transport and water retention capability in Nafion. Wang et al.[36] measured the tensile strength, water retention, swelling of the membrane, and conductivity of the composite membranes and concluded that the composite membranes perform better than Nafion in terms of mechanical properties. GO has been incorporated in several other composite membranes, such as sulfonated polyether ketone,[37] polybenzimidazole,[38] and polyvinyl.[39] Bayer et al.[40] studied the electrical and mechanical properties of GO membranes and provided a comparison with the conventional Nafion membrane. The authors reported water retention to be higher in GO as compared to Nafion, which is desired for higher conductivity. Kumar et al.[41] characterized several Nafion/GO composites by scanning electron microscopy and transmission electron microscopy. The authors attributed the enhanced proton conductivity to interactions between the different functional groups in GO and Nafion. Also, the authors concluded that the incorporation of GO enhances the mechanical stability without affecting the swelling properties of the membrane.

The study of the ion and water diffusion characteristics under confined conditions formed in porous polymeric materials attracts the interest of academic society and industry from different scientific perspectives.[42] The formation of the experimentally observed Nafion nanochannels can be promoted in simulations by the presence of GO. Although there have been several experimental investigations on Nafion/GO composites, to our knowledge, there has been no computational study reported so far. Hence, in the present study, we employ classical MD simulations to examine the nanostructure of Nafion/GO composites at various hydration levels and also the diffusion of water molecules and hydrated protons. Although classical MD simulations cannot describe the

DOI: 10.1021/acs.jpcc.8b07170
J. Phys. Chem. C 2018, 122, 22864−22875

Grotthuss diffusion of protons, these simulations can reveal the interplay between the two hydrophilic centers, Nafion and GO, and the surface polymer dynamics at different distances from the nanosheet. In this study, we calculated various properties such as (a) density profiles along the GO sheet, (b) density distribution of different species normal to the GO plane, (c) average dimensions and shape characteristics of Nafion chains, (d) orientational order of Nafion, water, and hydronium, (e) intermolecular radial distribution functions (RDFs), (f) cluster analysis of water molecules, (g) non-Gaussian parameter (NGP) of water and hydronium ions, (h) desorption autocorrelation functions of hydronium ions from GO, and (i) mean square displacement (MSD) of water and hydronium ions. The computational details are presented in Section 2. The results and discussion are presented in Section 3. A summary of key findings concludes this paper.

2. SIMULATION PROTOCOL

Each of the simulated Nafion GO nanocomposites (referred to as NAFGO henceforth) contains 100 polymer chains of 10 monomers each (Figure 1a), (m = 10 and n = 7, where m describes the degree of polymerization and n stands for the length of a monomer, see Figure 1b in ref 43) and 1 sheet of GO. The parameters and charge distribution for Nafion and hydronium were based on the optimized potentials for liquid simulations all-atom (OPLS-AA) force field[21,43,44] and are shown in Table S1 and Scheme S1 of the Supporting Information. GO had lateral dimensions of 8.5 × 8.1 nm^2 (initial/energy-minimized configuration shown in Figure 1b) and was surface modified to attain a carbon-to-oxygen ratio of 5:1 and a hydroxyl-to-epoxy group ratio of 3:2.[45] The GO sheet was constructed using basic unit flakes with dimensions of 1.5 nm × 2 nm as shown in ref 46, where the hydroxyl and the epoxy groups were placed randomly (in numbers commensurate to the target carbon-to-oxygen ratio) in each side of the flake. These units were repeated (with varying orientations and occasionally flipped over) to form the final GO sheet. In this way, the correct carbon-to-oxygen ratio is maintained while the level of randomness increases with respect to that of the basic unit. Hydrogen atoms were added to the edge carbon atoms. The partial charges and atomic interaction parameters were derived from the OPLS-AA force field.[44,47] The force field parameters of GO are shown in Table S2 of the Supporting Information. The inclusion of the nanosheet resulted in a Nafion membrane of 3.4 wt % in GO, which is close to the experimental values (of ∼4.0 wt %).[41] The choice of one large nanosheet allowed a ratio of GO lateral dimensions to Nafion dimensions closer to the experimental values.

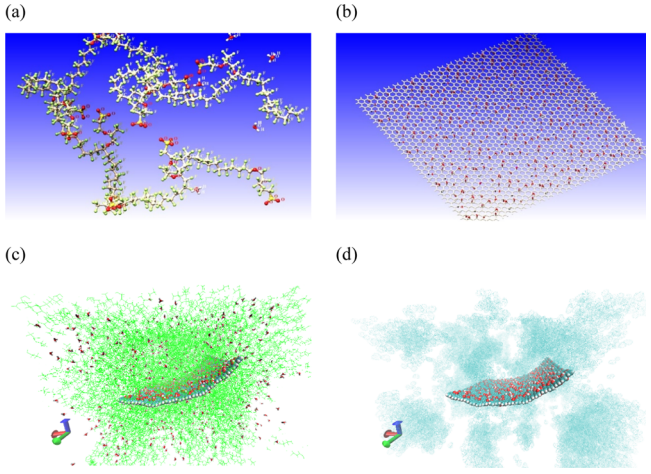

Figure 1. (a) One 10-mer fully ionized Nafion chain with respective hydronium ions, (b) GO with epoxy and hydroxyl groups (red points represent oxygens and white represents hydrogens), (c) equilibrated Nafion/hydronium/GO system at λ = 10 (water is not shown for clarity), and (d) the same as in (c) but showing only GO and water molecules. The origin of the coordinates system used [low left side of pictures (c,d)] was the GO CM.

The water concentration (hydration level) is defined by the parameter λ, which is equal to the number of water molecules per side chain pendant of Nafion. The water concentrations chosen in this study are λ = 10, λ = 15, and λ = 20. At these water concentrations, all sulfonate groups are fully ionized, and to maintain charge neutrality of the system, corresponding equal number of hydronium ions was added[43] (see Figure 1a). As a reference, we have performed simulations in the absence of GO, with 15 Nafion chains and the respective hydronium and water molecules (referred to as NAF from now on). Moreover, we have also simulated as the reference system (of two different sizes) pristine water, parametrized using the extended simple point charge (SPC/E) model.[48]

The initial configurations of the NAFGO and NAF systems were initially equilibrated for 80 ns at 1000 K to allow an efficient sampling in the adsorbed Nafion layer.[21] At this temperature, water molecules were not included, where as in the NAFGO system, GO was kept frozen (the thermostat was only applied to Nafion chains and hydronium ions). Then, the system containing the Nafion/hydronium ions was cooled to 600 K. At this temperature, a common thermal treatment was adopted for all molecules, by subjecting them to a cooling of 50 K/30 ns to reach the target temperature of 350 K. At 350 K, water molecules were introduced in the system, depending on the choice of water concentration. Similar cooling rates were used for systems to reach temperatures of 300 and 250 K. For all target temperatures (250, 300, and 350 K), an MD equilibration of 30 ns and a production run of several hundred ns were performed to allow the calculation of the diffusion coefficients of water molecules and hydronium ions. Gromacs software 5.1.4 package[49] was utilized for the creation of initial configurations and MD runs. The simulations were performed with the isobaric−isothermal (*NPT*) ensemble, using the isotropic Berendsen barostat,[50] with a target pressure of 1.0 bar, the compressibility parameter equal to 4.5 × 10^{-5} bar^{-1}, and the time constant for coupling equal to 0.5 ps. The temperature was controlled by the v-rescale thermostat[51] with a time constant equal to 0.2 ps. For the NAFGO systems, the short (vertical to the GO plane) z-dimension of the simulation box was almost 9 nm. This length is almost 75% of the length in the other two dimensions and represents the interplate distance. In the NAF systems, a cubic box was used with periodic boundary conditions. For the nanocomposite systems, after the insertion of the water molecules, the number of atoms are 105 804, 120 804, and 135 804 for λ equal to 10, 15, and 20, respectively. A typical run on 120 cores in a computing cluster in SURFsara (Amsterdam) produced 47 ns/day. Comparison of the translational mobility of water, at 350 K, between the reference NAF system with 15 Nafion chains and an additional larger one with 100 Nafion chains showed insignificant finite size effects.

DOI: 10.1021/acs.jpcc.8b07170
J. Phys. Chem. C 2018, 122, 22864−22875

3. RESULTS AND DISCUSSION

3.1. Structural Properties. In Figure 1c,d, snapshots of an equilibrated NAFGO system at λ = 10 and T = 300 K are depicted. As shown, Nafion forms cavities through which a continuum phase of liquid water is formed (Figure 1d), whereas GO assumes a slightly curved conformation. Curved GO nanosheets have also been observed in other computational and experimental studies.[47,52]

The density profile of the entire NAFGO system at 300 K and λ = 15 is presented in Figure 2 as a function of the distance

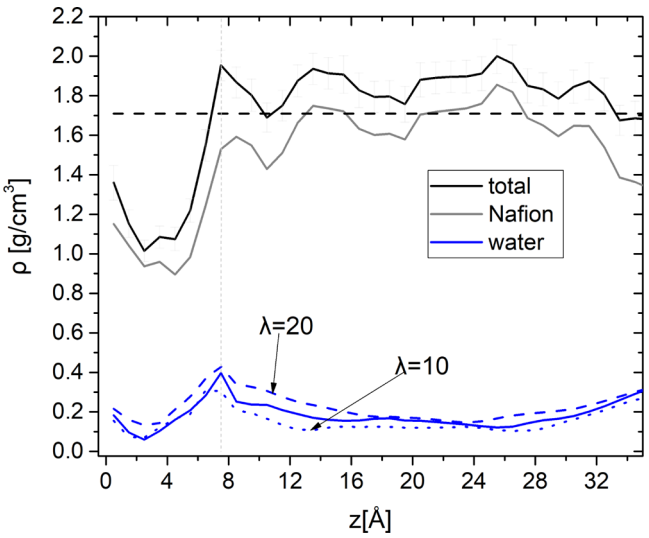

Figure 2. Density profiles along a direction perpendicular to the GO sheet as functions of the distance from the GO surface, for the NAFGO systems. The overall density, along with the contributions of Nafion and water, at T = 300 K and λ = 15 is presented. Additionally, for water, we also present the cases of λ = 10 (blue dot line) and λ = 20 (blue dash line).

from the GO plane. Only for water, we also compare with the cases of the other two hydration levels equal to 10 and 20. The bin size was set to 1 Å. The density of the respective NAF system, at the same temperature and hydration level, is denoted with a horizontal black dashed line. The vertical dotted line is a guide for the eye and determines the first adsorbed layer.

In all cases, the distance of a moiety (atom or molecule) from GO was taken as the magnitude of the projection of the vector connecting the moiety [or its center of mass (CM) if this was a molecule] and the GO CM to the vector normal to the GO plane (z-axis). Because the fluctuation in the GO shape can be realized in a statistical manner from both sides of the GO sheet (i.e., sometimes slightly overestimating and others underestimating the distances from the GO plane), it is expected that the GO curvature results, on average, only in a minor error in the estimated distances. At each time frame, a local coordinate system based on the gyration tensor of the GO sheet was utilized for the determination of the GO orientation. Moreover, to avoid the influence of the outer regions of GO, we present results taking into account atoms with X and Y coordinates lying within a rectangle with dimensions not exceeding 80% of the X and Y dimensions of GO. This treatment can be considered to represent the case of a macroscopic-sized GO sheet. Also, it allows the exclusion of the outer regions, which may assume a different curvature.

A depletion layer in the total density profile can be observed at distances shorter than 7.5 Å, where a peak in the density is present. Ensuing this maximum, a minimum close to 10 Å distance is clearly seen in the total and in the NAF profiles. Similar density profiles were also observed in the previous MD study[53] for low hydrophilicity substrates. This behavior remains essentially the same for all λ levels examined, depicting only somewhat stronger fluctuations for λ = 10. The peak at 7.5 Å is augmented by the increase in the concentration of water, as implied by the water profile, and is verified for all λ, as shown in the same figure. This peak should not be mistaken to represent a universal behavior of water near GO, but, as will be explained later, is related to the structure of Nafion chains close to the GO surface. For λ equal to 20, an increase in the concentration of water close to the GO is observed.

The number densities of the CMs for the three types of molecules, normalized by the corresponding overall averages, as functions of the distance from the GO plane, are depicted in Figure 3. The results refer to λ = 15 and T = 300 K, as shown in Figure 2.

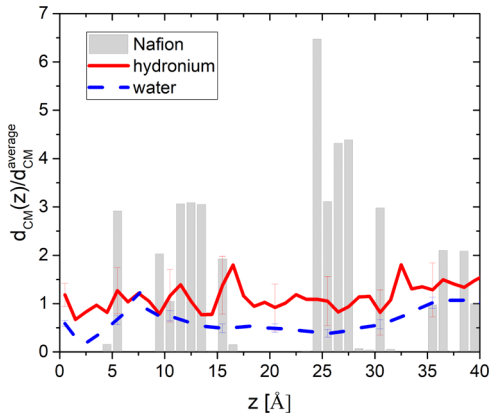

Figure 3. Normalized number density distributions of the CMs in the direction normal to the GO plane for the three molecular types in the NAFGO system at λ = 15 and T = 300 K.

The behavior concerning water follows closely those described by the density profiles in Figure 2. Close to the GO surface, water exhibits a value below unity, followed by a minimum at a distance of approximately 2.5 Å. Hydronium, on the other hand, shows on average an almost constant profile along the direction normal to GO. The fluctuations in the number density of hydronium close to GO were more intense at the lower hydration level examined. Concerning the CMs of the Nafion chains, a depletion region close to GO is observed. The existence of layers parallel to GO with zero concentration in Nafion is consistent with the immobilization of the backbone of the chains at temperatures below 350 K, at least within a time window of about 300 ns that was explored here. The discontinuity in the distribution of the CMs of Nafion reveals the formation of channels of average size equal to almost 6 Å. The sharp peaks reaching intensities up to 6.5 attest to the increased heterogeneities in the distribution of the Nafion chains within the composite membranes.

In Figure 4 we examine the shape characteristics and the average dimensions of the Nafion chains, through the evaluation of the principal moments of the gyration tensor of the Nafion chains, as a function of their distance from the GO plane. The results presented refer to the system at λ = 15 and

DOI: 10.1021/acs.jpcc.8b07170
J. Phys. Chem. C 2018, 122, 22864−22875

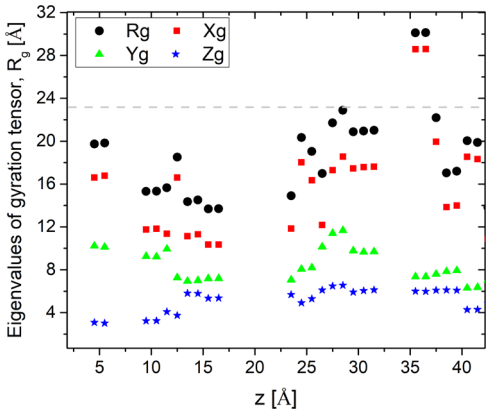

Figure 4. Radius of gyration (black circles) of the Nafion chains as a function of the distance from the GO plane. The eigenvalues of the gyration tensor in descending order (X_g/red squares, Y_g/green triangles, and Z_g/blue stars) are shown as well. The horizontal dashed line denotes the radius of gyration of the Nafion chains in the reference bulk NAF system. The standard deviation compared to the values is presented in Figure S1 in the Supporting Information.

T = 300 K; we note that the results are representative for the other hydration levels and temperatures as well. It is shown that the chains are characterized by average radii of gyration (R_g)[54] somewhat smaller compared to those in the bulk (this is more prominent at layers close to GO).

Because the number of counts of each eigenvalue in each layer is the same, the standard deviation may give us a rough estimate regarding the size of the fluctuations in each direction of the Nafion shape ellipsoid as a function of the distance from the GO plane. As depicted in Figure S1 in the Supporting Information section, the fluctuations in slabs close to GO are somewhat higher for the two smaller eigenvalues (Y_g, Z_g). This picture is consistent with the rather immobilized, adsorbed backbones of Nafion chains with more mobile side groups. Moreover, the asphericity (Figure S2 in the Supporting Information) calculated based on the difference between the highest eigen value and the average of the two smaller ones[54] supports the idea that in layers close to GO, the shape of the chain tends to have reduced values of R_g and is more spherical. The small curvature of the GO nanosheet (Figure 1c,d), may also have affected the shape of the adsorbed Nafion chains. At longer distances from GO, the highest eigenvalue, X_g, takes values that trigger an increase of the asphericity and the dimensions of the polymer coil.

The magnitude of the Nafion backbone end-to-end vector and that of the side chain vector are depicted in Figure S3 in the Supporting Information. Comparison of the lengths of the backbone and the side chains of Nafion with the average R_g values may offer information concerning the most common conformation of the adsorbed Nafion layer. Close to GO, the polymer chains exhibit an extended backbone, reaching values close to 40 Å, whereas the side chains take values lower than 7 Å. Only the length of the side chains does show a significant standard deviation. In the neighboring layers, until the distance of about 15 Å from the GO surface, the observed values imply reduced backbone dimensions. The length of the side chain was found to be between 6.8 and 7.0 Å in agreement with previous works.[53,55] Moreover, this length is comparable to the distance at which the depletion layer was observed in Figure 3. This picture suggests that part of the hydrophilic side chains adsorb on GO excluding the Nafion backbone, whereas the remaining associated with water molecules give rise to the peak in the water number density at 7.5 Å (as can be seen in Figures 2 and 3). These results support a picture of structured layers of the Nafion backbone parallel to the GO surface,[56] with the hydrophilic mobile side chains contributing to the formation of the water channels.

To examine the degree of backbone and side chain orientational ordering, we calculated the second-order Legendre polynomial of the backbone and side chain vectors, taking as reference axis (θ = 0) the direction vertical to GO.

$$P_2(\cos\theta) = \langle(3\cos^2\theta - 1)/2\rangle \quad (1)$$

A zero value describes the case of no orientational order, a value of 1 represents the case of parallel to the reference axis orientation, and a value of −0.5 describes vertical to the reference axis orientation. The results are presented in Figure 5.

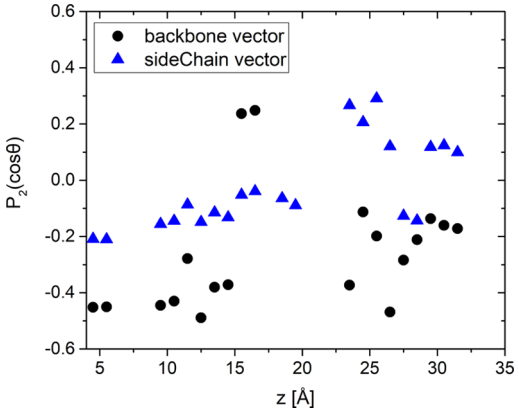

Figure 5. Orientational order parameter of the backbone/end-to-end vector (CT−CT, black circles) and the side chain vector (SY−CT, blue triangles) at λ = 15 and T = 300 K.

The backbone vector is defined as the end-to-end vector between the backbone carbons, CT−CT, whereas the side chain vector is defined as the vector between the backbone carbon and sulfur, CT−SY (see Table S2 for the list of the different atom types). It is shown that the Nafion backbone vector is almost parallel to GO at distances up to about 15 Å, whereas at longer distances, the orientation of the Nafion chain backbone is on average lower. On the other hand, the hydrated side chains are less ordered[53] probably due to their coupling to the more mobile water molecules. Small negative values are only present in the region of 0−15 Å from the surface. The overall picture described in Figures 3−5 implies the presence of a partial structure/order rather than the semicrystallization of the Nafion chains.[57]

An important characteristic of the Nafion membrane structure is the sulfur−sulfur (SY−SY) RDF.[55] Properties such as channel width and conductivity are related to this RDF. Figure 6 depicts the SY−SY pair RDF at 300 K at three different hydration levels.

The results for the NAFGO systems (solid lines) are compared with the respective NAF reference systems (dashed lines). At λ = 10, both NAF and NAFGO systems show a clear peak at approximately 5.3 Å. At higher hydration levels, the intensity of this peak drops significantly at the NAF systems, probably due to an increased mobility induced by the higher water percentage. This argument is supported by the picture

DOI: 10.1021/acs.jpcc.8b07170
J. Phys. Chem. C 2018, 122, 22864−22875

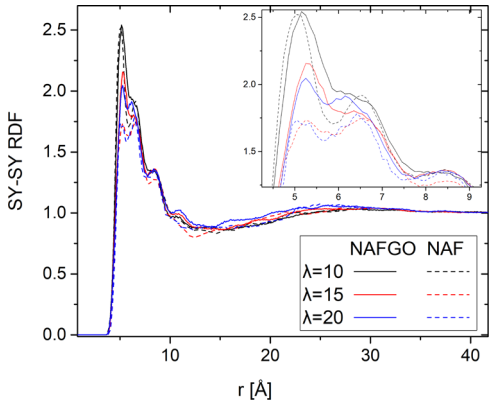

Figure 6. Pair RDF for the sulfur−sulfur atoms of the Nafion chains at 300 K at the three studied hydration levels. The inset shows a magnification of the main panel.

characterizing the NAFGO systems; the intensity drop at the main correlation peak at the higher λ values is lower compared to that in the respective NAF systems. The behavior observed in the NAFGO systems can be rationalized by the hydrophilicity of GO. Although the nanofiller does not trigger extensive adsorption of water, it does attract hydronium ions that are solvated by water and also adsorbs a few percentage of water molecules, thereby inhibiting the delocalization of the sulfur groups.

Next, we examine the orientation of the hydronium and water molecules utilizing an order parameter analogous to that described by eq 1. In this case, from the gyration tensor of each molecule/ion, we calculate the eigenvalues and the respective eigenvectors. The orientational order parameter of the eigenvectors related to the higher eigenvalues of the hydronium ions and water molecules, with respect to the direction normal to the GO surface, is shown in Figure 7.

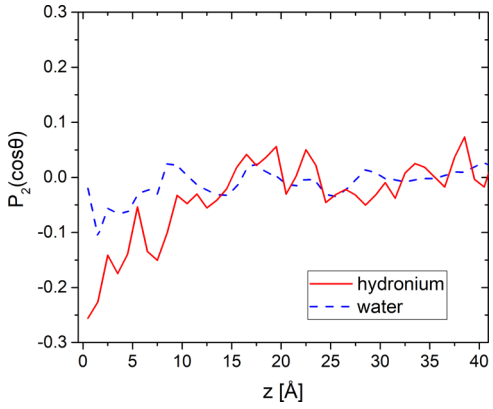

Figure 7. Orientational order parameter of the eigenvectors of the highest eigenvalues with respect to the vector normal to the GO plane, for the hydronium (red solid line) and water (blue dash line) molecules at T = 300 K and λ = 15.

It is shown that the hydronium ions assume negative order parameter values, which correspond to an orientation parallel to GO. At distances higher than 15 Å, the hydronium ions become less affected by the nanofiller and the structure of the Nafion backbone, exhibiting no orientational order. Therefore, it follows closely the behavior shown by the backbone vector (Figure 5). On the other hand, water molecules exhibit a rather low orientational order even close to GO. The lowest value of −0.1 is attained just after the adsorbed layer of the hydronium ions (Figure 3). The behavior remains the same in the other two cases of hydration levels, whereas the fluctuations in the order parameter of hydronium become more intense at T = 250 K and λ = 10. The adsorbed hydronium ions are affected by the concentration and mobility of water, whereas water molecules that solvate the adsorbed hydroniums follow the ordering of the latter close to GO.

3.2. Water Cluster Analysis. The clustering behavior of water is directly related to the morphology of the channels formed in the Nafion-based membranes. It is therefore of interest to study certain aspects of this behavior as a function of the hydration level and the temperature. For this purpose, we have carried out a cluster formation analysis utilizing the DBSCAN algorithm,[58] which is a density-based algorithm that detects clusters with an arbitrary shape and in the presence of noise. Each water molecule was considered as a single point represented by its CM. The basic idea of this cluster detection algorithm is that for each particle in a cluster, the neighborhood of a given radius ε (the so-called ε-neighborhood) has to contain at least a minimum number of objects, N_{min}. In other words, the ε-neighborhood of a water molecule, p, is defined by $N_\varepsilon(p) = \{q \in D | \text{ distance } (p,q) \leq \varepsilon\}$, where D denotes the database of the objects (here the set formed by the CM of water molecules in the simulation box). If for an arbitrary water molecule p, $N_\varepsilon(p) > N_{min}$, then this molecule can be considered as a "core point" from which the cluster growth can be initiated. In our case, we have taken N_{min} = 2, whereas ε was determined from the location of the first peak of the water−water pair correlation function (see Figure S7 in the Supporting Information) to be 2.8 Å. Although several variations of this method have been described in the literature (see ref 59), we believe that the main features of the clustering behavior of water molecules can be captured by the basic algorithm.[60] For comparison purposes, we have used as a reference for each temperature the behavior of the corresponding pure water systems.

Figure 8 shows the size distribution of water clusters formed in the examined systems at a hydration level of λ = 15. The clustering behavior of pure water at the same temperatures is

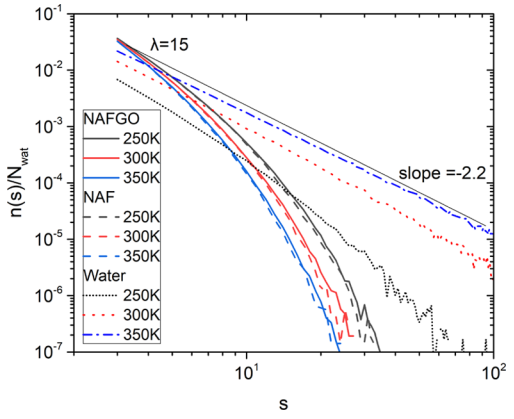

Figure 8. Number of formed clusters, $n(s)$, normalized by the total number of water molecules, N_{wat}, included in each system as a function of the cluster size, s, at λ = 15 for the NAFGO and NAF systems. Corresponding distributions for pure water systems are shown for comparison. The solid straight line denotes a power law behavior with an exponent of −2.2 (see text).

DOI: 10.1021/acs.jpcc.8b07170
J. Phys. Chem. C 2018, 122, 22864−22875

also shown for comparison. Clearly, the clustering behavior of water molecules in the Nafion membranes at all temperatures deviates significantly from its behavior in the corresponding pristine water systems. This picture also characterizes the behavior in the other two hydration levels examined (see Figure S8 in the Supporting Information). At high temperatures, the cluster distributions in pure water follow a power law, which is in close agreement with the universal exponent of −2.2, predicted by the Fisher droplet model[61] in the subcritical region. As temperature lowers and the percolation threshold of the water network is approached, the cluster distribution in pristine water deviates progressively from this power law. To check for finite size effects, we have also examined much larger water systems (about 10 times larger box volume). No significant changes in the observed behavior were noted (see Figure S9 in the Supporting Information).

The behavior in the Nafion-based systems, however, does not follow a single power law even at the highest temperature examined, indicating that the water cluster growth mechanism changes drastically once Nafion is introduced. The presence of GO does not seem to alter appreciably the characteristics of the cluster distributions observed in the NAF systems. In the latter systems, the distributions drop faster as the temperature increases compared to the behavior in pure water, resulting in a drastically smaller number of large-sized clusters. This practically means that the interconnectivity of water molecules (which would have led to the formation of a higher number of larger-sized water clusters) is hindered as the temperature rises. This, in turn, indicates that the water-percolated structure, which promotes conductivity in the membranes,[26,62] is deteriorated rapidly as the temperature increases. If we take into account all of the formed clusters (independently of their size), the general trend is that the number of clusters decreases with temperature (with or without the presence of GO, see Figure S10 in the Supporting Information).

On the other hand, at a constant temperature, the curves of the water cluster distributions exhibit a somewhat stronger drop when decreasing the hydration level, as shown in Figure 9. The effect of hydration on the distributions is more pronounced at the larger-sized clusters for all temperatures and becomes less important as the temperature increases (see Figure S11 in the Supporting Information).

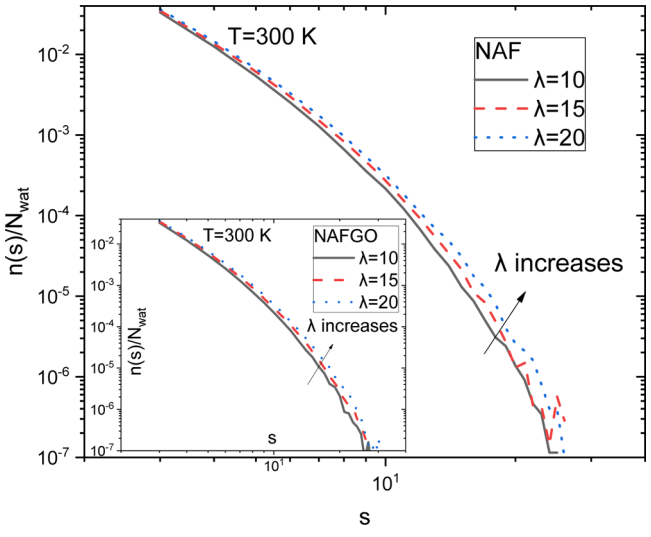

Figure 9. Dependence of the water cluster distributions (defined as in Figure 8) on the hydration level at constant T = 300 K. The main panel describes the behavior of the NAF membranes and the inset that of the NAFGO systems.

3.3. Dynamic Properties. Dynamic properties of the examined models were resolved at different distances (layers) with respect to the GO platelet. The CM of a molecule participated in the layer analysis only if the latter resided within that layer, both at the time of origin (t = 0) and at time t. In addition, only CMs of hydronium ions and water molecules whose X and Y projections were located within the X−Y boundaries of the GO sheet were taken into account.

Figure 10 displays the MSD of the CMs of water and hydronium ions, at λ = 15 and T = 300 K. We distinguished

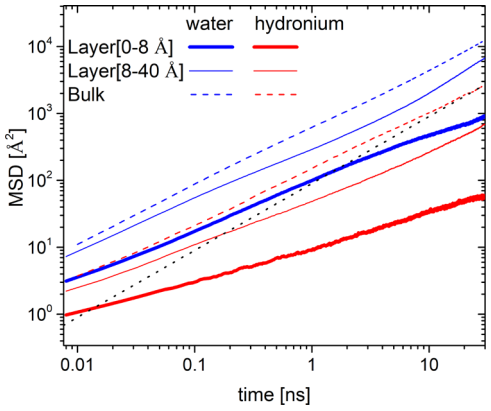

Figure 10. Planar component of the MSD of water and hydronium CMs in the two first layers adjacent to GO for the NAFGO system at λ = 15 and T = 300 K. Blue thick, thin, and dashed lines describe the results for water, whereas the red thick, thin, and dashed lines refer to hydronium ions. The black dashed line denotes the 3D Fickian behavior.

the two layers based on the first maximum in the density profile, as shown in Figure 2. In the first layer, the molecules are considered adsorbed as they are located in-between the GO and the first Nafion layer, whereas in the second layer, they are expected to move through the Nafion channels. The displacement was projected to the coordinate system of GO. We have focused on the X and Y (planar) components of the MSD; to be able to compare with the three-dimensional (3D) diffusion in the NAF systems (where all X, Y, and Z components participate in the MSD), the planar components were appropriately scaled (the average of the two components of the in-plane diffusion was multiplied by a factor of 3 to account for the difference in dimensionality[42]).

A general trend is that the dynamics in the Nafion/GO interface becomes slower compared to the corresponding NAF systems.[63,64] Examination of the analogous behavior at λ = 10 and λ = 20 (not shown here) confirms a layer close to GO with decelerated dynamics. This is the case not only for the heavier hydronium ions but also for the water molecules residing in the first layer close to GO. In the second layer, both water molecules and hydronium ions restore part of their mobility that was lost in the first layer, but the degree of speed-up is lower for the hydronium ions. The reason for this slowdown in the Nafion channels at the second adsorption layer might be related to the presence of the GO surface because hydronium ions taken to belong to the second layer could have visited the first layer (where dynamics is slower) at intermediate times.

DOI: 10.1021/acs.jpcc.8b07170
J. Phys. Chem. C 2018, 122, 22864−22875

Nevertheless, the average MSD in the whole NAFGO systems depicts that the dynamics tends to restore at high λ.

To quantify the mobility contrast between the components at different hydration levels, the diffusion coefficients (D) of the CMs were evaluated at T = 300 K for the nanocomposite and reference systems. For the hydronium ions, the calculated values for the NAFGO (and NAF) systems were 0.03 (0.04), 0.07 (0.08), and 0.12 (0.16) in units of 10^{-5} cm^2/s for λ levels equal to 10, 15, and 20, respectively. For water molecules at the NAFGO (and NAF) systems, the diffusion coefficients of the CM were evaluated to be 0.17 (0.31), 0.35 (0.52), and 0.53 (0.68) in units of 10^{-5} cm^2/s for hydration levels equal to 10, 15, and 20, respectively. Previous studies of the motion of a penetrant molecule in a porous media have demonstrated an "anomalous" behavior at short times.[64] This makes the identification of the Fickian regime ambiguous and might result in discrepancies in the estimation of D.[64] In our case, the diffusion coefficient of water under bulk conditions at T = 300 K was calculated to be 2.9 × 10^{-5} cm^2/s.[48]

Figures 11 and 12 depict the results of hydronium and water related to the NGP, $\alpha_2(t)$, of the CMs, defined as

$$\alpha_2(t) = \frac{3\langle \Delta r(t)^4 \rangle}{5\langle \Delta r(t)^2 \rangle^2} - 1 \quad (2)$$

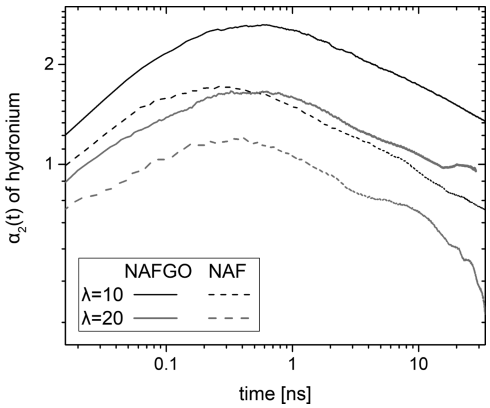

Figure 11. NGP of the CMs of hydronium ions at λ = 10 and 20 and T = 300 K for both nanocomposite and bulk.

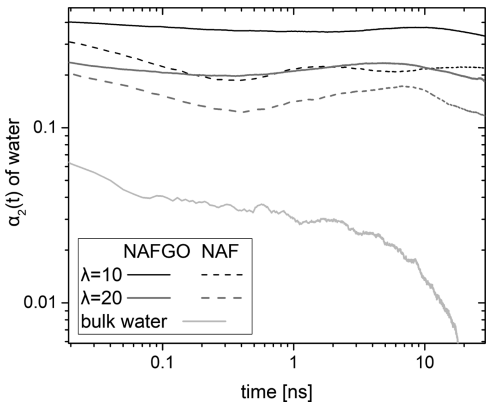

Figure 12. NGP of the CMs of water molecules at λ = 10 and λ = 20 and T = 300 K in the nanocomposite, in the Nafion/water, and in the pristine (bulk) water systems.

Parameter $\alpha_2(t)$[65] takes the minimum theoretical value (−0.4) when all CMs travel the same displacement; value 0 describes Brownian diffusion, whereas values greater than 0 appear when the distances traveled after time t by the particles under examination are not Gaussian distributed.

In the case of hydronium ions, at 300 K in the NAFGO systems, the NGP is higher compared to the respective reference systems and increases as λ drops. The curve for the NAFGO systems at λ = 10 exhibits a maximum value, which is shifted toward longer times compared to the behavior in NAF. This indicates a higher degree of confinement of hydronium ions in the composite systems, in line with their partial adsorption onto the GO surface, as discussed earlier. On the other hand, as shown in Figure 10, water undergoes significantly less heterogeneous diffusion at the same temperature. The trend for an increase in the degree of motional heterogeneity in the nanocomposite systems compared to the reference systems and a decrease of $\alpha_2(t)$ as λ increases is also present. Nevertheless, the values of $\alpha_2(t)$ for water are an order of magnitude lower compared to the values of hydronium ions. This notion corroborates the differences observed in the diffusion coefficients quoted earlier.

Next, we focus on the dynamics related to the adsorption/desorption mechanism of the hydronium ions from the GO surface, as this procedure is important for the apparent conductivity of the nanocomposite membrane. To this end, we have evaluated the appropriate dynamic correlation functions described by the equation[46]

$$h(t) = \frac{\langle g(t)\, g(0) \rangle}{\langle g^2 \rangle} \quad (3)$$

We have taken as the adsorption criterion the critical distance of 3.7 Å between the hydroxyl hydrogen of GO and the oxygen of hydronium, which corresponds to the first peak of the respective pair RDF function (not shown here). In this context, $g(t)$ assumes a value of 1 for any examined pair, if this pair satisfies the criterion at time t, and 0 otherwise. The angle brackets denote averaging over all pairs and time origins. The critical distance is practically the same as in the case of the sulfur−hydronium interaction.

To describe the results and make an extrapolation to longer times, we have fitted the correlation functions describing the desorption dynamics by means of the modified Kohlrausch−Williams−Watts (mKWW) expression[66]

$$P(t) = \alpha_1 \exp\left[-\frac{t}{\tau_1}\right] + (1 - \alpha_1) \exp\left[-\left(\frac{t}{\tau_2}\right)^{\beta}\right] \quad (4)$$

The mKWW fitting function assumes a Debye (first term) and a stretch exponential relaxation (second term) that is in agreement with the idea[45] of the existence of both Arrhenius and non-Arrhenius components in complex dynamics. On the basis of the fitting parameters and the expression for the decorrelation time, $\tau_c = a_1\tau_1 + (1 - a_1)\left(\frac{\tau_2}{\beta}\right)\Gamma\left(\frac{1}{\beta}\right)$ where Γ is the gamma function and the desorption times are evaluated to be 5 × 10^7, 6 × 10^6, and 1 × 10^6 ns for hydration levels λ = 10, λ = 15, and λ = 20, respectively. The results (Figure 13) emphasize the significance of the hydration level on the hydronium interfacial dynamics. At λ = 10, the desorption time is an order of magnitude larger compared to those at higher hydration levels. Only at λ = 20, the cations desorb from GO at times close to 1 ms. We mention that the average residence time of the water and hydronium ions on the sulfur group of

DOI: 10.1021/acs.jpcc.8b07170
J. Phys. Chem. C 2018, 122, 22864−22875

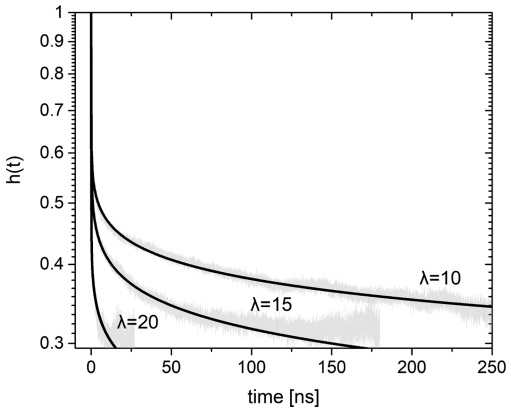

Figure 13. Desorption autocorrelation function (eq 3) of the oxygen (Oh) of hydronium ions from the hydrogen (hO) of the GO hydroxyl.

the Nafion is of the order of picosecond and nanosecond, respectively,[19] although cases of hydronium bound to SO_3^- for longer times (approximately 1 ms) have also been detected.[19] The deviation in desorption times between GO and Nafion sulfur groups should be attributed to the low concentration of water near GO, especially at the hydration levels of $\lambda = 10$ and $\lambda = 15$. Because the hydronium ion undergoes restricted diffusion close to the nanosheet, it seems as if the Nafion side chains retain the necessary water for diffusion to take place. Nevertheless, a stricter comparison of the dynamics between the NAF membranes and the nanocomposites with GO would require the definition of an equivalent λ' hydration parameter that would also take into account the hydrophilic centers on GO.

Structural relaxation processes related to the translational motion of molecules, which take place within specific spatial dimensions can be described by the self-part of the intermediate scattering function as[65]

$$F_s(q, t) = \langle \exp(i\vec{q}\cdot[\vec{r}_i(t) - \vec{r}_i(0)]) \rangle \quad (5)$$

In Figure 14, we present the results based on the motion of the CM of water molecules in pristine water and in the two extreme hydration levels studied. As the evaluation of the dynamics close to the Fickian regime at $T = 250$ K is rather

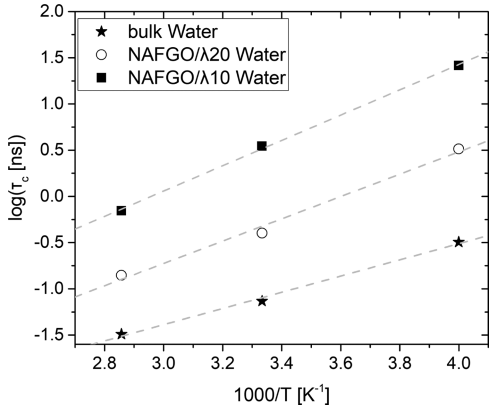

Figure 14. Decorrelation times of the incoherent dynamic structure factor (eq 5), $q = 0.22$ Å^{-1}, for water molecules (see text) at 300 K and 1 bar. The different symbols refer to the bulk state in the NAFGO/λ = 20 system and the NAFGO/λ = 10 system.

ambiguous, especially for the NAFGO systems, we have chosen to probe the water translational dynamics at a wave vector representing a length scale commensurate with the dimensions of the simulation box, that is, $q = 0.22$ Å^{-1}.[67]

Evidently, water becomes significantly slower in the Nafion nanocomposite membranes. The differences in the decorrelation times (always evaluated through eq 4), compared to the NAF reference systems, follow trends similar to those observed in the behavior of the CM diffusion coefficients. These results indicate that the channels formed by Nafion obstruct the diffusion of water with or without the presence of GO. The fitting to the Arrhenius part of eq 4 was better for the NAFGO/λ = 10 systems, whereas the activation energies were calculated to be 7.3, 10.0, and 11.3 kJ/mol for pure water, NAFGO/λ = 20, and NAFGO/λ = 10 systems, respectively.

In previous work,[42] it has been argued that highly confined conditions may promote diffusion with Arrhenius characteristics for the ions in the center of the pore. This kind of confinement could be realized in the mobile regions of semicrystalline polymer membranes or due to the presence of nanoparticles. In this study, although the partial structure of the Nafion backbone close to the GO nanosheet and an Arrhenius-like diffusion of water at short time scales were verified, no indications of crystallization were observed.[57] It is possible that an even larger GO sheet could allow the observation of such well-structured Nafion channels even within the time window that can be probed with fully atomistic MD simulations. Recent simulational studies on Nafion membranes[53,68] supported the idea of accelerated dynamics at the interface. According to that work, a highly attractive surface under capped/confined[69] conditions could create less tortuous water paths and in-plane hydronium ion diffusion. The particles forming the wall were represented by a crude Lennard-Jones 9/3 potential that does not introduce the roughness of the surface. Nevertheless, the introduction of wall forces parallel to the plane reduces the mobility at least at short times.[69−71]

Comparing our work, where a fully atomistic representation of the GO nanosheet was adopted, with the previous study of Nafion confined by wall potentials,[53] it can be concluded that except for the attraction strength of the wall, another parameter that drastically determines the hydrophilicity of the nanosheet is the surface roughness. Conditions that can promote a bound form of water or just restrictions in the mobility of the adsorbed water are not favorable at room temperature. Besides, high water adsorption levels on GO would dehydrate Nafion inhibiting diffusion in the formed channels while resulting in a large reduction in the entropy of the entire system. So, the introduction of hydrophilicity by hydroxyl and epoxy groups that restrict in-plane diffusion may explain with thermodynamic arguments the decreased water adsorption compared to other simulated systems.[53] A smoother nanosheet with less surface roughness and the same interaction strength may also exhibit higher degree of water adsorption. Finally, the study supports the idea that GO in the NAFGO systems starts to withhold water only when Nafion is well-hydrated ($\lambda > 15$), accelerating the hydronium ion adsorption/desorption process.

4. CONCLUSIONS

In this work, we have examined for the first time by means of fully atomistic molecular dynamics simulations, nanocomposite membranes comprised by Nafion and GO at different

DOI: 10.1021/acs.jpcc.8b07170
J. Phys. Chem. C 2018, 122, 22864−22875

hydration levels of the Nafion chains and at different temperatures. The same membranes without the presence of GO as well as pristine water models were used as reference systems.

From the structural analysis of the composite systems, it was found that close to the GO surface, layers of Nafion were formed with the chain backbones oriented parallel to the GO plane. Close to the interface, Nafion assumes somewhat smaller chain dimensions with different shapes compared to those in the GO-free systems. The hydrophilic side chains, on the other hand, assume an average size and orientation, which essentially facilitate the formation and determine the spatial dimensions of the water channels through their hydrated sulfur groups. Part of the hydronium ions were found to adsorb onto the GO surface, exhibiting an enhanced orientational order. The degree of localization of the hydronium ions close to the GO sheet increased with the decreasing hydration level, which resulted in longer time scales of the relevant adsorption/desorption process.

The mechanism for water cluster formation was strongly affected upon introduction of Nafion (with or without the presence of GO), compared to that in the pristine water systems. More specifically, the number of larger-sized water clusters dropped dramatically, and the cluster growth mechanism deviated strongly from the single-exponent power law characterizing the pure water systems at high temperatures. Upon increasing the temperature, the number of large-sized clusters decreased significantly. At a constant temperature, the effect of hydration level on the cluster size distribution was rather small, but anyhow more important for the larger-sized clusters.

From the dynamic point of view, the structural relaxation due to the translational motion of water in the composite systems was found to slow down compared to that realized in pristine water, apparently due to the presence of the hydronium ions and the higher degree of confinement of the water molecules. The degree of slowing down was considerably higher in the layer immediately adjacent to GO. The increase of the hydration level resulted in the speed-up of water dynamics because the degree of confinement decreased. At all hydration levels examined, the water translational motion exhibited Arrhenius-like behavior with increasing activation energies as the hydration level dropped. This behavior will be explored in more detail in a future work where dynamics inside the formed channels will be described with spatial and temporal resolutions.

The aforementioned detailed structural and dynamic characteristics of the different components forming the Nafion-based composite membranes can be used as a first step toward a better understanding of the processes related to the formation of the interconnected channels, which essentially determine the conductivity of such membranes as well as other physical properties (such as structural integrity, water retention capacity, etc.) associated with their overall performance.

■ ASSOCIATED CONTENT

Supporting Information

The Supporting Information is available free of charge on the ACS Publications website at DOI: 10.1021/acs.jpcc.8b07170.

Force field of Nafion, force field parameters for GO, ratio of the standard deviation of Nafion, asphericity of Nafion, lengths of the backbone and side chain vectors, Oh−OW RDF, Oh−SY RDF, OW−SY RDF, water−water RDF, number of water clusters, comparison of the pure water cluster distribution for different box sizes, percentage of water participating in clusters, and comparison of water cluster distribution in the Nafion membranes (PDF)

■ AUTHOR INFORMATION

Corresponding Authors

*E-mail: kritikgio@cheng.auth.gr (G.K.).
*E-mail: karatas@eng.auth.gr (K.K.).

ORCID

Georgios Kritikos: 0000-0003-2579-6597
Soumyadipta Sengupta: 0000-0003-3814-1741
Arun Venkatnathan: 0000-0001-8450-5417
Alexey V. Lyulin: 0000-0002-7533-3366

Notes

The authors declare no competing financial interest.

■ ACKNOWLEDGMENTS

The work has been performed under the Project HPC-EUROPA3 (INFRAIA-2016-1-730897), with the support of the EC Research Innovation Action under the H2020 Programme. G.K. gratefully acknowledges the support of the host group "Theory of Polymers and Soft Matter" at TUe and the computer resources and technical support provided by the HPC Access Centre SURFsara. K.K. would like to thank FO.R.T.H-IESL for the warm hospitality during his stay there. R.P. thanks the Indian Institute of Science Education and Research, Pune, for the graduate fellowship. A.V. is thankful to the DST Nanomission Thematic Unit (SR/NM/TP-13/2016) for the financial support toward this work.

■ REFERENCES

(1) Devanathan, R. Recent Developments in Proton Exchange Membranes for Fuel Cells. *Energy Environ. Sci.* **2008**, *1*, 101−119.
(2) Zawodzinski, T. A.; Derouin, C.; Radzinski, S.; Sherman, R. J.; Smith, V. T.; Springer, T. E.; Gottesfeld, S. Water Uptake by and Transport Through Nafion 117 Membranes. *J. Electrochem. Soc.* **1993**, *140*, 1041.
(3) Bass, M.; Berman, A.; Singh, A.; Konovalov, O.; Freger, V. Surface Structure of Nafion in Vapor and Liquid. *J. Phys. Chem. B* **2010**, *114*, 3784−3790.
(4) Goswami, S.; Klaus, S.; Benziger, J. Wetting and Absorption of Water Drops on Nafion Films. *Langmuir* **2008**, *24*, 8627−8633.
(5) Economou, N. J.; Barnes, A. M.; Wheat, A. J.; Schaberg, M. S.; Hamrock, S. J.; Buratto, S. K. Investigation of Humidity Dependent Surface Morphology and Proton Conduction in Multi-Acid Side Chain Membranes by Conductive Probe Atomic Force Microscopy. *J. Phys. Chem. B* **2015**, *119*, 14280−14287.
(6) Noguchi, H.; Taneda, K.; Minowa, H.; Naohara, H.; Uosaki, K. Humidity-Dependent Structure of Surface Water on Perfluorosulfonated Ionomer Thin Film Studied by Sum Frequency Generation Spectroscopy. *J. Phys. Chem. C* **2010**, *114*, 3958−3961.
(7) Kwon, O.; Kang, Y.; Wu, S.; Zhu, D.-M. Characteristics of Microscopic Proton Current Flow Distributions in Fresh and Aged Nafion Membranes. *J. Phys. Chem. B* **2010**, *114*, 5365−5370.
(8) McLean, R. S.; Doyle, M.; Sauer, B. B. High-Resolution Imaging of Ionic Domains and Crystal Morphology in Ionomers Using AFM Techniques. *Macromolecules* **2000**, *33*, 6541−6550.
(9) Novitski, D.; Holdcroft, S. Determination of O2 Mass Transport at the PtPFSA Ionomer Interface under Reduced Relative Humidity. *ACS Appl. Mater. Interfaces* **2015**, *7*, 27314−27323.

DOI: 10.1021/acs.jpcc.8b07170
J. Phys. Chem. C 2018, 122, 22864−22875

(10) Tang, J.; Yuan, W.; Zhang, J.; Li, H.; Zhang, Y. Evidence for a Crystallite-Rich Skin on Perfluorosulfonate Ionomer Membranes. *RSC Adv.* **2013**, *3*, 8947−8952.
(11) Vishnyakov, A.; Neimark, A. V. Molecular Dynamics Simulation of Microstructure and Molecular Mobilities in Swollen Nafion Membranes. *J. Phys. Chem. B* **2001**, *105*, 9586−9594.
(12) Paddison, S. J. The Modeling of Molecular Structure and Ion Transport in Sulfonic Acid Based Ionomer Membranes. *J. New Mater. Electrochem. Syst.* **2001**, *4*, 197−207.
(13) Paddison, S.; Elliott, J. The effects of backbone conformation on hydration and proton transfer in the short-side-chain perfluorosulfonic acid membrane. *Solid State Ionics* **2006**, *177*, 2385−2390.
(14) Agmon, N. The Grotthuss Mechanism. *Chem. Phys. Lett.* **1995**, *244*, 456−462.
(15) Jang, S. S.; Molinero, V.; Çağin, T.; Goddard, W. A. Effect of Monomeric Sequence on Nanophase-Segregated Structure and Water Transport in Nafion 117. *Am. Chem. Soc., Div. Fuel Chem., Prepr. Pap.* **2003**, *48*, 510−511.
(16) Urata, S.; Irisawa, J.; Takada, A.; Shinoda, W.; Tsuzuki, S.; Mikami, M. Molecular Dynamics Study of the Methanol Effect on the Membrane Morphology of Perfluorosulfonic Ionomers. *J. Phys. Chem. B* **2005**, *109*, 17274−17280.
(17) Venkatnathan, A.; Devanathan, R.; Dupuis, M. Atomistic Simulations of Hydrated Nafion and Temperature Effects on Hydronium Ion Mobility. *J. Phys. Chem. B* **2007**, *111*, 7234−7244.
(18) Devanathan, R.; Venkatnathan, A.; Dupuis, M. Atomistic Simulation of Nafion Membrane: I. Effect of Hydration on Membrane Nanostructure. *J. Phys. Chem. B* **2007**, *111*, 8069−8079.
(19) Devanathan, R.; Venkatnathan, A.; Dupuis, M. Atomistic Simulation of Nafion Membrane. 2. Dynamics of Water Molecules and Hydronium Ions. *J. Phys. Chem. B* **2007**, *111*, 13006−13013.
(20) Cui, S.; Liu, J.; Selvan, M. E.; Keffer, D. J.; Edwards, B. J.; Steele, W. V. A Molecular Dynamics Study of a Nafion Polyelectrolyte Membrane and the Aqueous Phase Structure for Proton Transport. *J. Phys. Chem. B* **2007**, *111*, 2208−2218.
(21) Sunda, A. P.; Venkatnathan, A. Molecular Dynamics Simulations of Side Chain Pendants of Perfluorosulfonic Acidpolymer Electrolyte Membranes. *J. Mater. Chem. A* **2013**, *1*, 557−569.
(22) Petersen, M. K.; Wang, F.; Blake, N. P.; Metiu, H.; Voth, G. A. Excess Proton Solvation and Delocalization in a Hydrophilic Pocket of the Proton Conducting Polymer Membrane Nafion. *J. Phys. Chem. B* **2005**, *109*, 3727−3730.
(23) Petersen, M. K.; Voth, G. A. Characterization of the Solvation and Transport of the Hydrated Proton in the Perfluorosulfonic Acid Membrane Nafion. *J. Phys. Chem. B* **2006**, *110*, 18594−18600.
(24) Feng, S.; Voth, G. A. Proton Solvation and Transport in Hydrated Nafion. *J. Phys. Chem. B* **2011**, *115*, 5903−5912.
(25) Ilhan, M. A.; Spohr, E. Hydrogen Bonding in Narrow Protonated Polymer Electrolyte Pores. *J. Electroanal. Chem.* **2011**, *660*, 347−351.
(26) Schmidt-Rohr, K.; Chen, Q. Parallel Cylindrical Water Nanochannels in Nafion Fuel-Cell Membranes. *Nat. Mater.* **2008**, *7*, 75−83.
(27) Büchi, F. N. Operating Proton Exchange Membrane Fuel Cells Without External Humidification of the Reactant Gases. *J. Electrochem. Soc.* **1997**, *144*, 2767.
(28) Pourzare, K.; Mansourpanah, Y.; Farhadi, S. Advanced Nanocomposite Membranes for Fuel Cell Applications: A Comprehensive Review. *Biofuel Res. J.* **2016**, *3*, 496−513.
(29) Lee, D. C.; Yang, H. N.; Park, S. H.; Kim, W. J. Nafion/Graphene Oxide Composite Membranes for Low Humidifying Polymer Electrolyte Membrane Fuel Cell. *J. Membr. Sci.* **2014**, *452*, 20−28.
(30) Karim, M. R.; Hatakeyama, K.; Matsui, T.; Takehira, H.; Taniguchi, T.; Koinuma, M.; Matsumoto, Y.; Akutagawa, T.; Nakamura, T.; Noro, S.-i.; Hayami, S.; et al. Graphene Oxide Nanosheet with High Proton Conductivity. *J. Am. Chem. Soc.* **2013**, *135*, 8097−8100.
(31) Zarrin, H.; Higgins, D.; Jun, Y.; Chen, Z.; Fowler, M. Functionalized Graphene Oxide Nanocomposite Membrane for Low Humidity and High Temperature Proton Exchange Membrane Fuel Cells. *J. Phys. Chem. C* **2011**, *115*, 20774−20781.
(32) Devanathan, R.; Chase-Woods, D.; Shin, Y.; Gotthold, D. W. Molecular Dynamics Simulations Reveal That Water Diffusion between Graphene Oxide Layers Is Slow. *Sci. Rep.* **2016**, *6*, 29484.
(33) Liu, G.; Jin, W.; Xu, N. Graphene-Based Membranes. *Chem. Soc. Rev.* **2015**, *44*, 5016−5030.
(34) Choi, B. G.; Huh, Y. S.; Park, Y. C.; Jung, D. H.; Hong, W. H.; Park, H. S. Enhanced Transport Properties in Polymer Electrolyte Composite Membranes with Graphene Oxide Sheets. *Carbon* **2012**, *50*, 5395−5402.
(35) Enotiadis, A.; Angjeli, K.; Baldino, N.; Nicotera, I.; Gournis, D. Graphene-Based Nafion Nanocomposite Membranes: Enhanced Proton Transport and Water Retention by Novel Organo-Functionalized Graphene Oxide Nanosheets. *Small* **2012**, *8*, 3338−3349.
(36) Wang, L.; Kang, J.; Nam, J.-D.; Suhr, J.; Prasad, A. K.; Advani, S. G. Composite Membrane Based on Graphene Oxide Sheets and Nafion for Polymer Electrolyte Membrane Fuel Cells. *ECS Electrochem. Lett.* **2014**, *4*, F1−F4.
(37) Jiang, Z.; Zhao, X.; Fu, Y.; Manthiram, A. Composite Membranes Based on Sulfonated Poly(Ether Ether Ketone) and SDBS-Adsorbed Graphene Oxide for Direct Methanol Fuel Cells. *J. Mater. Chem.* **2012**, *22*, 24862−24869.
(38) Üregen, N.; Pehlivanoğlu, K.; Özdemir, Y.; Devrim, Y. Development of Polybenzimidazole/Graphene Oxide Composite Membranes for High Temperature PEM Fuel Cells. *Int. J. Hydrogen Energy* **2017**, *42*, 2636−2647.
(39) Rudra, R.; Kumar, V.; Pramanik, N.; Kundu, P. P. Graphite Oxide Incorporated Crosslinked Polyvinyl Alcohol and Sulfonated Styrene Nanocomposite Membrane as Separating Barrier in Single Chambered Microbial Fuel Cell. *J. Power Sources* **2017**, *341*, 285−293.
(40) Bayer, T.; Bishop, S. R.; Nishihara, M.; Sasaki, K.; Lyth, S. M. Characterization of a Graphene Oxide Membrane Fuel Cell. *J. Power Sources* **2014**, *272*, 239−247.
(41) Kumar, R.; Xu, C.; Scott, K. Graphite Oxide/Nafion Composite Membranes for Polymer Electrolyte Fuel Cells. *RSC Adv.* **2012**, *2*, 8777.
(42) Kritikos, G.; Vergadou, N.; Economou, I. G. Molecular Dynamics Simulation of Highly Confined Glassy Ionic Liquids. *J. Phys. Chem. C* **2016**, *120*, 1013−1024.
(43) Sengupta, S.; Pant, R.; Komarov, P.; Venkatnathan, A.; Lyulin, A. V. Atomistic Simulation Study of the Hydrated Structure and Transport Dynamics of a Novel Multi Acid Side Chain Polyelectrolyte Membrane. *Int. J. Hydrogen Energy* **2017**, *42*, 27254−27268.
(44) Jorgensen, W. L.; Maxwell, D. S.; Tirado-Rives, J. Development and Testing of the OPLS All-Atom Force Field on Conformational Energetics and Properties of Organic Liquids. *J. Am. Chem. Soc.* **1996**, *118*, 11225−11236.
(45) Kritikos, G.; Karatasos, K. Temperature Dependence of Dynamic and Mechanical Properties in Poly(Acrylic Acid)/Graphene Oxide Nanocomposites. *Mater. Today Commun.* **2017**, *13*, 359−366.
(46) Karatasos, K.; Kritikos, G. Characterization of a Graphene Oxide/Poly(Acrylic Acid) Nanocomposite by Means of Molecular Dynamics Simulations. *RSC Adv.* **2016**, *6*, 109267−109277.
(47) Tang, H.; Liu, D.; Zhao, Y.; Yang, X.; Lu, J.; Cui, F. Molecular Dynamics Study of the Aggregation Process of Graphene Oxide in Water. *J. Phys. Chem. C* **2015**, *119*, 26712−26718.
(48) Berendsen, H. J. C.; Grigera, J. R.; Straatsma, T. P. The Missing Term in Effective Pair Potentials. *J. Phys. Chem.* **1987**, *91*, 6269−6271.
(49) Hess, B.; Kutzner, C.; van der Spoel, D.; Lindahl, E. GROMACS 4: Algorithms for Highly Efficient, Load-Balanced, and Scalable Molecular Simulation. *J. Chem. Theory Comput.* **2008**, *4*, 435−447.
(50) Berendsen, H. J. C.; Postma, J. P. M.; van Gunsteren, W. F.; DiNola, A.; Haak, J. R. Molecular Dynamics with Coupling to an External Bath. *J. Chem. Phys.* **1984**, *81*, 3684−3690.

DOI: 10.1021/acs.jpcc.8b07170
J. Phys. Chem. C 2018, 122, 22864−22875

(51) Bussi, G.; Donadio, D.; Parrinello, M. Canonical Sampling through Velocity Rescaling. *J. Chem. Phys.* **2007**, *126*, 014101.
(52) Whitby, R. L. D.; Gun'ko, V. M.; Korobeinyk, A.; Busquets, R.; Cundy, A. B.; László, K.; Skubiszewska-Zięba, J.; Leboda, R.; Tombácz, E.; Toth, I. Y.; et al. Driving Forces of Conformational Changes in Single-Layer Graphene Oxide. *ACS Nano* **2012**, *6*, 3967−3973.
(53) Sengupta, S.; Lyulin, A. V. Molecular Dynamics Simulations of Substrate Hydrophilicity and Confinement Effects in Capped Nafion Films. *J. Phys. Chem. B* **2018**, *122*, 6107−6119.
(54) Theodorou, D. N.; Suter, U. W. Shape of Unperturbed Linear Polymers: Polypropylene. *Macromolecules* **1985**, *18*, 1206−1214.
(55) Sunda, A. P.; Venkatnathan, A. Atomistic Simulations of Structure and Dynamics of Hydrated Aciplex Polymer Electrolyte Membrane. *Soft Matter* **2012**, *8*, 10827.
(56) Nagao, Y. Proton-Conductivity Enhancement in Polymer Thin Films. *Langmuir* **2017**, *33*, 12547−12558.
(57) Mauritz, K. A.; Moore, R. B. State of Understanding of Nafion. *Chem. Rev.* **2004**, *104*, 4535−4586.
(58) Ester, M.; Kriegel, H.-P.; Sander, J.; Xu, X. A Density-Based Algorithm for Discovering Clusters in Large Spatial Databases with Noise. *KDD-96 Proceedings*, 1996; Vol. *96*, pp 226−231.
(59) Rehman, S. U.; Asghar, S.; Fong, S.; Sarasvady, S. DBSCAN: Past, Present and Future. *The Fifth International Conference on the Applications of Digital Information and Web Technologies (ICADIWT 2014)*; IEEE, 2014; pp 232−238.
(60) Amini, A.; Wah, T. Y.; Saboohi, H. On Density-Based Data Streams Clustering Algorithms: A Survey. *J. Comput. Sci. Technol.* **2014**, *29*, 116−141.
(61) Fisher, M. E. The Theory of Condensation and the Critical Point. *Phys. Phys. Fiz.* **1967**, *3*, 255−283.
(62) Devanathan, R.; Venkatnathan, A.; Rousseau, R.; Dupuis, M.; Frigato, T.; Gu, W.; Helms, V. Atomistic Simulation of Water Percolation and Proton Hopping in Nafion Fuel Cell Membrane. *J. Phys. Chem. B* **2010**, *114*, 13681−13690.
(63) Siroma, Z.; Kakitsubo, R.; Fujiwara, N.; Ioroi, T.; Yamazaki, S.-i.; Yasuda, K. Depression of proton conductivity in recast Nafion film measured on flat substrate. *J. Power Sources* **2009**, *189*, 994−998.
(64) Karayiannis, N. C.; Mavrantzas, V. G.; Theodorou, D. N. Diffusion of Small Molecules in Disordered Media: Study of the Effect of Kinetic and Spatial Heterogeneities. *Chem. Eng. Sci.* **2001**, *56*, 2789−2801.
(65) van Megen, W.; Mortensen, T. C.; Williams, S. R.; Müller, J.; van Megen, W. Measurement of the self-intermediate scattering function of suspensions of hard spherical particles near the glass transition. *Phys. Rev. E: Stat. Phys., Plasmas, Fluids, Relat. Interdiscip. Top.* **1998**, *58*, 6073−6085.
(66) Kohlrausch, R. Theorie des elektrischen Rückstandes in der Leidener Flasche. *Ann. Phys.* **1854**, *167*, 179−214.
(67) Damasceno Borges, D.; Franco, A. A.; Malek, K.; Gebel, G.; Mossa, S. Inhomogeneous Transport in Model Hydrated Polymer Electrolyte Supported Ultrathin Films. *ACS Nano* **2013**, *7*, 6767−6773.
(68) Sengupta, S.; Kritikos, G.; Karatasos, K.; Venkatnathan, A.; Pant, R.; Komarov, P.; Lyulin, A. V. Novel Polyelectrolyte Membranes for Fuel and Flow Batteries: Insights from Simulations. *AIP Conf. Proc.* **2018**, *1981*, 020004.
(69) Kritikos, G.; Sgouros, A.; Vogiatzis, G. G.; Theodorou, D. N. Molecular Dynamics Study of Polyethylene under Extreme Confinement. *J. Phys.: Conf. Ser.* **2016**, *738*, 012012.
(70) Zhu, Y.; Granick, S. Viscosity of Interfacial Water. *Phys. Rev. Lett.* **2001**, *87*, 096104.
(71) Gordillo, M. C.; Martí, J. Effect of Surface Roughness on the Static and Dynamic Properties of Water Adsorbed on Graphene. *J. Phys. Chem. B* **2010**, *114*, 4583−4589.

DOI: 10.1021/acs.jpcc.8b07170
J. Phys. Chem. C 2018, 122, 22864−22875